Parallel equilibrium current effects on the existence of reversed shear Alfvén eigenmodes

Hua-sheng Xie[1, *] and Yong Xiao[1, †]

[1]*Institute for Fusion Theory and Simulation, Department of Physics,*
Zhejiang University, Hangzhou, 310027, People's Republic of China
(Dated: July 30, 2014)

A new fast global eigenvalue code, where the terms are segregated according their physics, is developed to study Alfvén modes in tokamak plasmas, particularly, the reversed shear Alfvén eigenmode (RSAE). Numerical calculations show that the parallel equilibrium current corresponding to the kink term is unfavorable for the existence of the RSAE. An improved criterion for the RSAE existence is given for with and without the parallel equilibrium current. In the limits of ideal magnetohydrodynamics (MHD) and zero-pressure, the toroidicity effect is the main possible favorable factor for the existence of the RSAE, which is however usually small. This suggests that, suppression of the kink term in the simulation will help to find RSAE.

I. INTRODUCTION

In toroidal plasmas, the discrete shear Alfvén eigenmodes (AEs) can exist. These modes can be destabilized by fast particles and can therefore degrade the confinement[1]. Recently, a specific AE, namely, the reversed shear Alfvén eigenmode (RSAE), usually localized around the minimum value of the safety factor q (q_{min}) for a reversed shear tokamak plasma, has been intensively studied in experiments[2–7]. The frequency of the RSAE mode usually sweeps up or down when q_{min} drops in time. It also provides an indirect method for measuring the safety factor profile[3]. Hence, it is important to study the properties of the RSAE.

The present work is inspired by a recent experiment in the HL-2A tokamak[8]. Under that RSAE experimental parameters, NOVA[9] cannot find the RSAE mode[8]. However, the KAEC code[10] seems can find an eigenmode as in the experiment by excluding the kink term or including kinetic effects. The existence of RSAEs has also been studied intensively theoretically, including the effects of energetic particle[11], toroidicity[12], finite plasma pressure[13–15], pressure gradient[16, 17], density gradient[18], as well as some kinetic effects[10, 19]. The effect of the parallel equilibrium current corresponding to the kink term has also been studied recently by Deng *et al.*[20, 21] using the GTC code and an analytical model for the dispersion relation, where the toroidal coupling is ignored.

In the literatures, three different approaches have been employed to study Alfven eigenmodes, particularly, the RASE. The first approach is to solve a reduced model equation analytically, usually a 1D eigenvalue equation (e.g., [22]). The second is to solve a more complicated model equation numerically by finding its eigenvalues and eigenfunctions (e.g., [9]). The third is to use large scale simulation to solve a more general set of equations (e.g., [20]).

In this paper, all these three approaches are used to study RSAE. Firstly, we provide a set of coupling AE equations for toroidal plasmas that retains the exact self-adjointness of the original ideal magnetohydrodynamic (MHD) equation, and is not limited to large toroidal and poloidal mode numbers. Then, a fast global eigenvalue code, namely, AMC (Alfvén Mode Code) is developed, to calculate the Alfvén continuum spectrums and the frequencies and mode structures of AEs, which can be used effectively to benchmark other large simulation codes. Finally, we apply this new code to study the parallel equilibrium current effect on RSAEs in detail. An improved criterion is found for the RSAE existence for both with and without the parallel equilibrium current. Numerical and analytical results show that the parallel equilibrium current is unfavorable for the existence of the RSAE. This explains why the aforementioned NOVA studies of the HL-2A experiment cannot find RASE easily since they include the parallel current automatically.

The paper is organized as follows. Sec. II describes the formalism and numerical scheme for the linear ideal MHD vorticity equation. Sec. III solves the preceding equation and discusses the importance of the parallel current in finding RSAE in both theory and simulation. Summary and discussion are given in Sec. IV.

II. MODEL AND FORMALISM

We start from the linearized ideal MHD vorticity equation[12, 14–16, 23]

$$\nabla \cdot \left[\frac{\omega^2}{v_A^2(r,\theta)} \nabla_\perp U \right] + \boldsymbol{B} \cdot \nabla \left(\frac{1}{B^2} \nabla \cdot B^2 \nabla_\perp Q \right) - \nabla \left(\frac{J_\parallel}{B} \right) \cdot (\nabla Q \times \boldsymbol{B}) + 2 \frac{\boldsymbol{\kappa} \cdot (\boldsymbol{B} \times \nabla \delta P)}{B^2} = 0, \quad (1)$$

where the stream function U is defined from plasma displacement vector using $\boldsymbol{\xi} = (\nabla U \times \boldsymbol{b})/B$, $\boldsymbol{\kappa} = \boldsymbol{b} \cdot \nabla \boldsymbol{b} = (\nabla \times \boldsymbol{b}) \times \boldsymbol{b}$ is the magnetic field curvature, $\boldsymbol{b} = \boldsymbol{B}/B$ is

the unit equilibrium magnetic field, $J_\parallel = (c/4\pi)\boldsymbol{b}\cdot\nabla\times\boldsymbol{B}$ is the parallel equilibrium current, $Q = (\boldsymbol{b}\cdot\nabla U)/B$, and $\delta P = (\boldsymbol{b}\times\nabla U\cdot\nabla P)/B + (\Gamma P\nabla U\cdot\boldsymbol{b}\times\boldsymbol{\kappa})/B$ with $\Gamma P = P_e + 7P_i/4$ to correctly treat the effective geodesic compressibility[14, 22]. Eq.(1) holds for a large aspect ratio ($\epsilon = r/R_0 \ll 1$) tokamak plasma to second order, and we have assumed low beta $\beta \sim O(\epsilon^2)$. The first term is the inertial term, the second term is the field line bending term, the third term is kink term and the last one is ballooning term. In Eq.(1), each physics term is well separated thus it is more convenient for physics studies than the original set of MHD equations, such as the equations used by NOVA[9] and GTAW[24]. Note that, since the electrostatic potential $\delta\phi$ is related to U by $\delta\phi = \partial U/\partial t$, therefore, the mode structure of U is also similar to that of $\delta\phi$.

Similar to Ref. [12, 14, 16], we consider a shifted circular flux surface equilibrium. The flux surface is defined by the usual cylindrical coordinate (R, ϕ_c, Z)

$$R = R_0 + r_s\cos\theta_s - \Delta(r_s), \tag{2a}$$
$$\phi_c = -\zeta_s, \tag{2b}$$
$$Z = r_s\sin\theta_s, \tag{2c}$$

where R_0 is the major radius and the Shafranov shift $\Delta(0) = 0$. The relations between flux coordinates (r, θ, ζ) and geometry coordinates (r_s, θ_s, ζ_s) are $r = r_s$, $\zeta = \zeta_s$ and $\theta = \theta_s - (\epsilon + \Delta')\sin\theta_s$, with Δ' being the radial derivative of the Shafranov shift $\Delta(r)$. Assuming $U = \sum U_m(r)\exp(in\zeta - im\theta)$ and expanding Eq.(1) to $O(\epsilon^2)$, we obtain a coupled equation

$$L_{m,m-1}U_{m-1} + L_{m,m}U_m + L_{m,m+1}U_{m+1} = 0, \tag{3}$$

where the operators $L_{m,m}$ and $L_{m,m\pm1}$ are defined as

$$L_{m,m} = \frac{\partial}{\partial r}\left[\frac{(1+4\epsilon\Delta')}{v_A^2}\bar\omega^2 - k_m^2 - c_s^2\right]r\frac{\partial}{\partial r} + (k_m^2)' -$$
$$\frac{m^2}{r}\left\{\frac{[1-4\epsilon(\epsilon+\Delta')]}{v_A^2}\bar\omega^2 - k_m^2 - c_s^2 - \bar\kappa_r\alpha/q^2\right\}, \tag{4}$$

$$L_{m,m\pm1} = \bar\omega^2\left\{\frac{\partial}{\partial r}\frac{(2\epsilon+\Delta')}{v_A^2}r\frac{\partial}{\partial r} - \frac{(\epsilon-\Delta')}{v_A^2}\frac{m(m\pm1)}{r}\right.$$
$$\left.\mp\frac{[\epsilon+(r\Delta')']}{v_A^2}m\frac{\partial}{\partial r}\right\} - \left\{\frac{\partial}{\partial r}r\Delta'k_mk_{m\pm1}\frac{\partial}{\partial r} - \right.$$
$$\frac{m^2}{r}(\epsilon+\Delta')k_mk_{m\pm1} \mp m[\epsilon+(r\Delta')']k_mk_{m\pm1}\frac{\partial}{\partial r}\right\}$$
$$-\frac{m\alpha}{2q^2}\left(\frac{m}{r}\mp\frac{\partial}{\partial r}\right). \tag{5}$$

Here, $\bar\omega = \omega/\omega_A$, $\omega_A = V_A/R_0$, $k_m = n - m/q$, $V_A = v_A(0)$ is the on-axis Alfvén velocity, $\alpha = -R_0q^2d\beta/dr$ is the normalized pressure gradient, $\bar\kappa_r = \epsilon(1/2 - 1/q^2) + (r\Delta')'/2 + \Delta'$ is the averaged radial component

of the curvature. The normalized ion-sound speed term $c_s^2 = [2/(V_A^2R_0^2)][T_e + (7/4)T_i]/m_i$ corresponding to the geodesic acoustic coupling can be calculated from kinetic theory[14, 22].

The above equations, which are improved from Ref.[12, 14, 16, 23, 25], recover the exact self-adjointness of ideal MHD equation and are also not limited to large toroidal and poloidal mode numbers. The detailed comparisons between our equations and those in other literatures are given in Appendix A. The proof of the self-adjointness is provided in Appendix B. This set of model equations supports a wide range of modes such as the Alfvén eigenmodes (Global AE, Toroidal induced AE, RSAE and more) and internal kink mode as well as ideal ballooning mode (IBM).

The above equations can be solved numerically for both continuum spectrums and eigenmodes. The continuum spectrums are obtained by setting the determinant of the coefficients of the second-order derivative terms to zero[26]. The eigenmodes are obtained by solving a matrix eigenvalue problem $\boldsymbol{AX} = \lambda\boldsymbol{BX}$, with $\omega^2 = \lambda$. The central difference scheme is used for the discretization of Eq.(3), $df/dr = (f_{j+1} - f_{j-1})/(2\Delta r)$ and $d^2f/dr^2 = (f_{j+1} - 2f_j + f_{j-1})/\Delta r^2$. The zero boundary conditions are used in the computation. The eigen matrix dimension is $(N_m \times N_r)^2$, where N_r is radial grid number and $N_m = m_{\max} - m_{\min} + 1$ is number of the m mode numbers, with $m \in [m_{\min}, m_{\max}]$ in the computation.

A new code named AMC is developed based on the above numerical scheme. To speed up computation, the sparse matrix method is used to calculated the eigenvalue (mode frequency) and eigenvector (mode structure). Compared to other codes (which usually use root finding scheme) such as NOVA[9], KAEC[10] and GTAW[24], this new code is easier to use and much faster to run. A typical run with $N_r = 512$ and $N_m = 10$, AMC can find an eigenmode in seconds or less, whereas NOVA and KAEC usually require minutes. Moreover, AMC can also calculate all the N_d ($N_d = N_r \times N_m$) eigenvalues and eigenvectors for the system in minutes, without losing solutions. Here, the eigenvalues contain both continuum and discrete spectrums. The mode structures are usually singular for the continuum spectrums at some radial locations, whereas the mode structures for the discrete spectrums are usually global and smooth, which are our main interests. The benchmarks of AMC are provided in Appendix C.

One should also note that although the triangularity and elongation have been excluded in our model, i.e., the $L_{m,m\pm2,3,\ldots}$ terms have been omitted in Eq.(3), the higher order continuum gaps (and AEs) may still exist, as can be seen in panels (b) in Figs.1 and 2. These higher order couplings occur in an indirect way, e.g., U_m could be coupled to U_{m+2} since U_m is directly coupled to U_{m+1} and U_{m+1} is also coupled to U_{m+2}.

III. PARALLEL EQUILIBRIUM CURRENT EFFECTS ON MODE EXISTENCE

In this paper, we study only the lowest order parallel equilibrium current effects for the RSAEs, which can be represented by the kink term in Eq.(1). For the case without the kink term, $L_{m,m}$ should be modified to $L_{m,m}^{\text{new}} = L_{m,m} - (3k_m k_m' + r k_m k_m'')$. Similar explicit expressions for the kink term are also obtained in Ref.[21, 25]. Note also that if the term $(k_m^2)'$ is missing in Eq.(4), the L_m^{new} would be inaccurate to be $L_{m,m}^{\text{new}} + 2k_m k_m'$.

Since RSAE is usually a single m dominant mode, following Ref.[11, 12, 14, 16], we can obtain the following dimensionless equation to manifest each physics term by simplifying and expanding Eq.(3) at the zero shear point,

$$\frac{\partial}{\partial x}(S + x^2)\frac{\partial}{\partial x}U_m + (Q - S - x^2)U_m = 0, \qquad (6)$$

where $x = m(r - r_0)/r_0$. Here and below, the subscript 0 represents the quantity at r_0, with r_0 being the radius at $q_{\min}$. The expression for S is unchanged from that in Ref.[14, 16]

$$S = \frac{mq_0^2}{(-k_{m0})r_0^2 q_0''}\left(\frac{\bar{\omega}^2}{v_{A0}^2} - k_{m0}^2\right), \qquad (7)$$

where we have ignored the compressibility term c_s^2 and Shafranov shift term. However, $Q = Q_{\text{tor}} + Q_{\text{pressure}}$ is changed to $Q = Q_{\text{tor}} + Q_{\text{pressure}} + Q_{\text{new}}$. We find that the improvement of L in our equations does not affect the Q_{tor} in Q, i.e.,

$$Q_{\text{tor}} = 2\frac{mq_0^2(-k_{m0})}{r_0^2 q_0''}\frac{(\epsilon^2 + 2\Delta'\epsilon)}{1 - 4k_{m0}^2 q_0^2}. \qquad (8)$$

This shows that the analysis of RSAE in Ref.[12, 14, 16] still holds, though their starting equation does not satisfy the self-adjointness and misses a $(k_m^2)'$ term. This is because that the main difference between the self-adjoint and non-self-adjoint L operator are the derivative term related to k_m', and $k_{m0}' = 0$ for RSAEs. The same holds for the $(k_m^2)'$ term, i.e., $(k_m^2)_0' = 0$. That is, the equations in Ref.[12, 14, 16] can be used for RSAEs, but, would be subtle for other AEs and other modes (e.g., internal kink and ballooning modes) when $k_m' \neq 0$, as mentioned in Appendix A.

Q_{new} is due to the absence of the kink term in Eq.(1). For the case with the kink term, $Q_{\text{new}} = 0$. For the case without the kink term,

$$Q_{\text{new}} \simeq \frac{r_0 k_{m0}(k_m'')_0}{r_0(k_m^2)_0''/2} \simeq 1. \qquad (9)$$

We note that Eq.(6) is much broader in application than ideal MHD modes. When dealing with fast particle driven or kinetic driven RSAEs modes, we simply replace the Q in Eq.(6) by $Q_{\text{eff}} = Q_{\text{f}} + Q_{\text{tor}} + Q_{\text{pressure}} + Q_{\text{kinetic}} +$

.... The existence of RSAEs requires $Q_{\text{eff}} > Q_{\text{critical}}$, with $Q_{\text{critical}} \simeq 1/4$[11] in general, where Q_{eff} depends on several factors, such as fast ion (Q_{f}), plasma pressure gradient (Q_{pressure}), toroidal coupling (Q_{tor}), kinetic effects (Q_{kinetic}), etc. Here, Q_{eff} can be understood as the Schrödinger potential, and $Q_{\text{eff}} > Q_{\text{critical}}$ can be understood similarly as the Suydam's criterion[11]. These terms can be either favorable or unfavorable. We find that for the case without the kink term, the Q_{new} in Eq.(9) is always larger than zero, which also makes easier $Q_{\text{eff}} > Q_{\text{critical}} = 1/4$. Therefore, the parallel equilibrium current is always an unfavorable effect. The above result is similar to the RSAE model equation by Deng *et al.*[20, 21]. However, in Deng's model equation, if the parallel equilibrium current is included, the RSAE will not exist; whereas in our equation the RSAE can still exist, as will be shown later. Nevertheless, one should keep in mind that the above analytical existence criteria $Q_{\text{critical}} = 1/4$ is not rigorous. Even in the current fluid limit, a more rigorous treatment needs to resort to numerical computation rather than the current analytic estimate.

Next, we verify the above conclusion numerically using the AMC code we developed. For simplicity, we focus on the zero-shift and zero-pressure limits, i.e., $\Delta(r) = 0$ and $\beta = 0$, which follows $c_s^2 = 0$ and $\alpha = 0$ (also $Q_{\text{pressure}} = 0$). Hereafter, if not specified, the frequency ω and the radius r are normalized by ω_A and minor radius a, respectively.

Firstly, the following reversed shear safety factor profile is chosen[27],

$$q(r) = q_m + c_1(r^2 - r_m^2)^2 + c_2(r^2 - r_m^2)^3, \qquad (10)$$

where $c_1 = [(q_a - q_m)r_m^6 + (q_0 - q_m)(1 - r_m^2)^3]/[r_m^4(r_m^2 - 1)^2]$ and $c_2 = [(q_a - q_m)r_m^4 - (q_0 - q_m)(1 - r_m^2)^2]/[r_m^4(r_m^2 - 1)^2]$. The Alfvén velocity profile related to the density profile is given by $v_A^2(r) = 1/\rho(r)$ and $\rho(r) = 1/(1 + 3r^2)$. The following parameters are chosen to calculate the RSAE mode structure: $n = 4$, $R_0/a = 5$, $q_m = 1.91$, $q_0 = 2.0$, $q_a = 3.5$ and $r_m = 0.5$.

The results for the two cases with and without the kink term are shown in Fig.1. The 1D and 2D mode structures in panels (c) and (d) of Fig.1 show that, for the case without the kink term, a fine global RSAE mode can be found. Whereas, for the case with the kink term, only a rough global mode can be found, as shown by panels (e) and (f) in Fig.1. So, the kink term is unfavorable for the existence of RSAE, which is consistent with our previous simple analytical model. Here, $Q_{\text{tor}} = 0.2578$ for our numerical parameters. We note that, although Q_{tor} is larger than the analytical critical value $1/4$, the global RSAE mode still doesn't exist well for $Q_{\text{new}} = 0$. This is because the analytical critical value $1/4$ is a crude estimate.

Secondly, it would also be interesting to see whether the pure toroidicity factor (i.e., $Q_{\text{f}} = Q_{\text{pressure}} = Q_{\text{kinetic}} = ... = 0$ but $Q_{\text{tor}} \neq 0$) can trigger RSAE in a global code. Our numerical calculations by the AMC
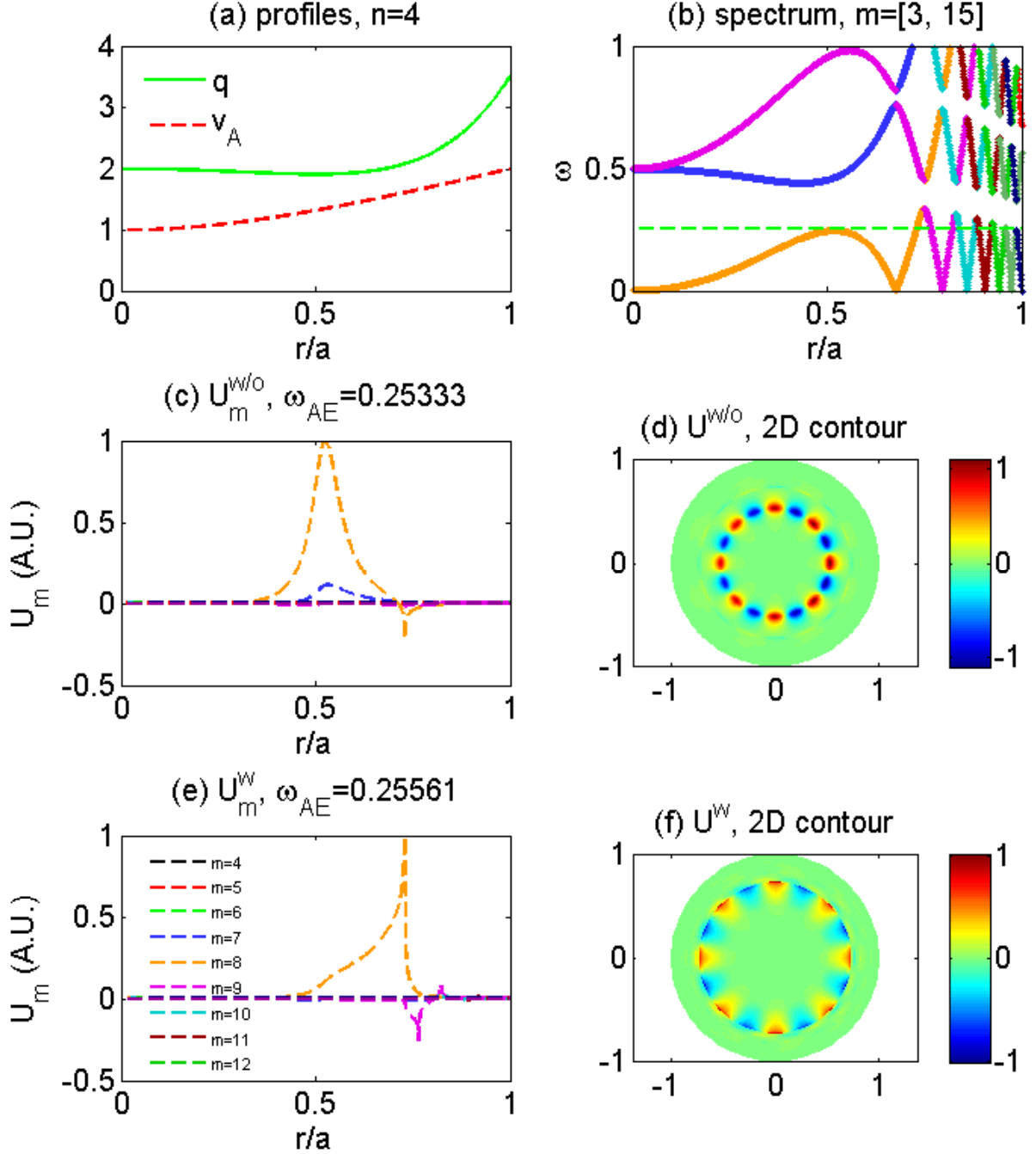
FIG. 1: The q-profile is Eq.(10) and $v_A^2(r) = 1 + 3r^2$. Under these parameters, a fine global RSAE mode only exist when the kink term is removed.

code show that it is possible although difficult.

The following q profile is chosen

$$q(r) = \frac{q_m}{[1 - (r - 0.5)^2/w_q^2]}, \qquad (11)$$

with $q_m = 1.87$ and $w_q = 2.5$. The toroidal mode number $n = 10$ is employed to make $Q_{\text{tor}} \gg Q_{\text{critical}} = 1/4$.

Fig.2 shows the RSAE mode structures for the cases with and without kink term. For both cases, a fine global

RSAE mode can be identified. And, the mode structures for both cases are similar except a slight difference in frequency. This indicates that the kink term mainly affects whether the RSAE can exist, but barely affects the mode structure with the existence of the RSAE. Since the terms in Q_{eff} are decoupled, Q_{new} can be used to mimic other physics effects, such as Q_f, Q_{kinetic}, to excite RSAE. In other words, we can suppress the kink term artificially to excite the RSAE. However, this method is only useful
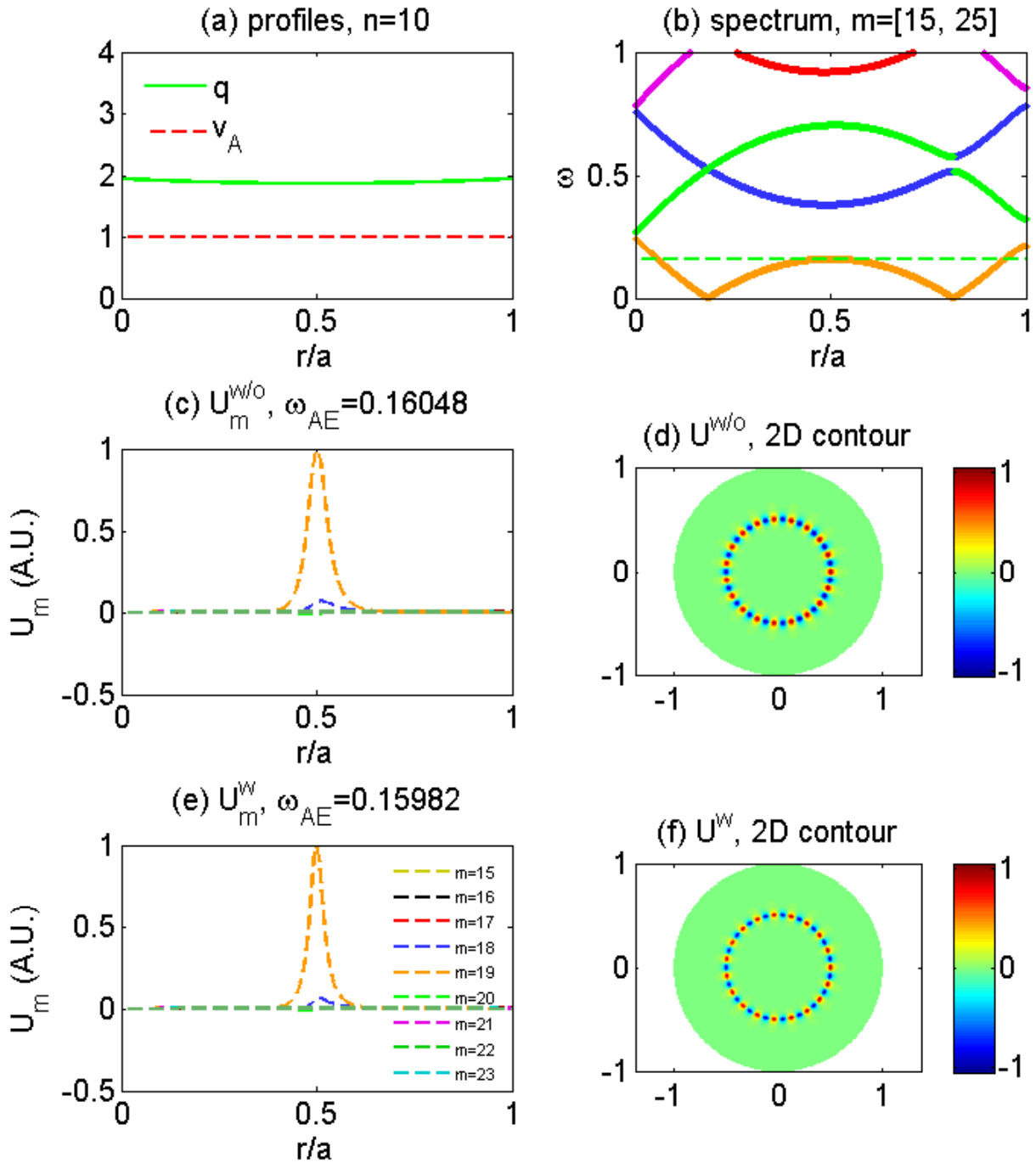
FIG. 2: The q-profile is Eq.(11) and $v_A^2(r) = 1$. A fine global RSAE mode exist for both cases with and without kink term.

for identifying the RSAE mode quickly.

A simulation verification is shown in Fig.3 using GTC code[21], where the q profile is given by $q = 1.948 - 0.31(\psi/\psi_w) + 0.31(\psi/\psi_w)^2$, with ψ the poloidal flux and $\psi_w = \psi(r = a) = 0.0105 B_0 R_0^2$, with B_0 the magnetic field at the magnetic axis. The corresponding $a/R_0 = 0.200$. The parameters are similar to that in Fig.2 and also yields $Q_{\text{tor}} \gg Q_{\text{critical}} = 1/4$ for $n = 10$. Fig.3 shows that a fine global RSAE mode can be found for both

cases. We have used the antenna to excite the eigenmode in this simulation to overcome the continuous damping and noise.

IV. SUMMARY AND DISCUSSION

In this study, we developed a fast eigenvalue code AMC to study Alfvén eigenmodes and ideal MHD instabili-
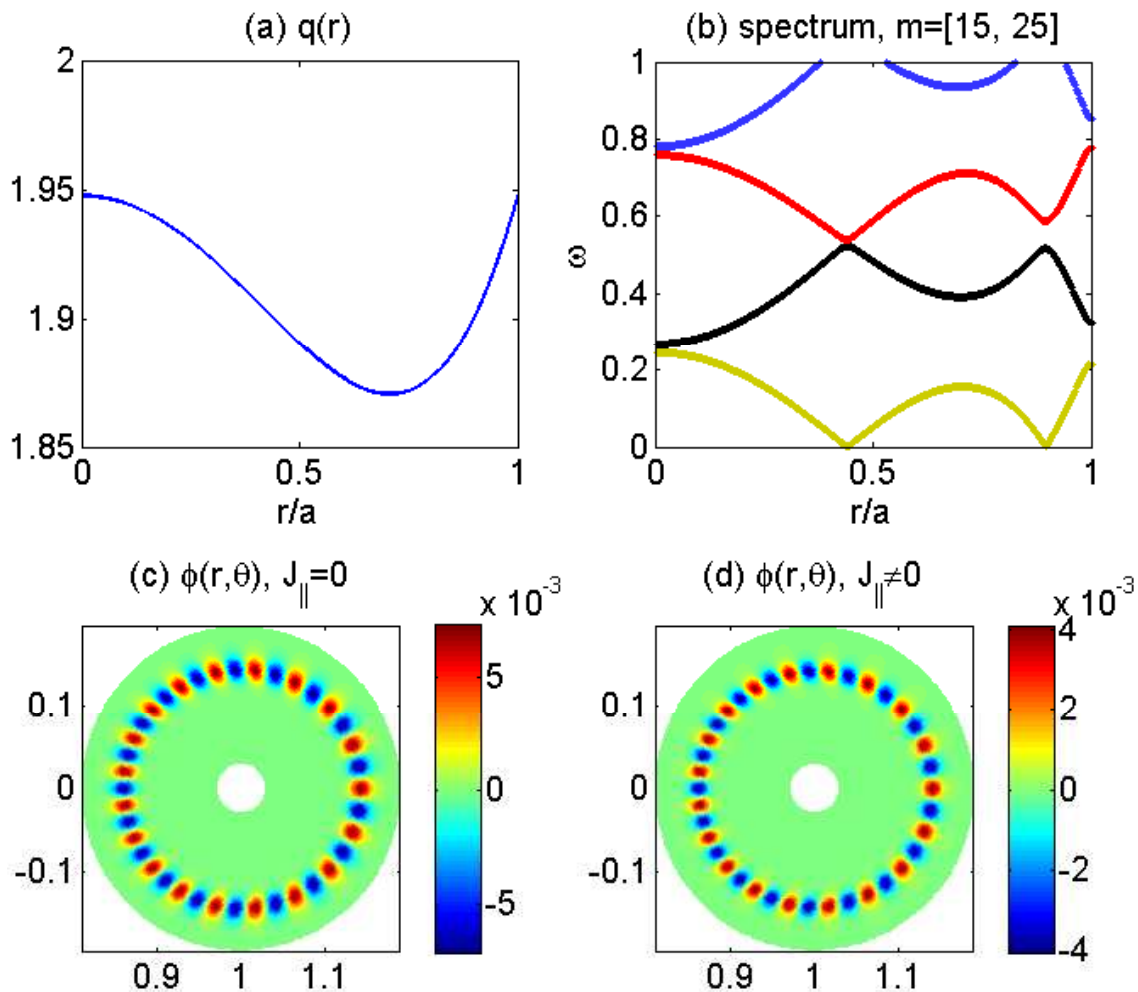
FIG. 3: GTC simulation of RSAE: (a) q(r) profile; (b & c) electrostatic potential ϕ on poloidal plane without and with kink term. Parameters: $n = 10$, $R_0/a = 5.0$, $q_{\min} = 1.87$. Under these parameters, RSAE exists for both with and without parallel equilibrium current cases.

ties in tokamaks. By using this code, we verified that the equilibrium parallel current contribution Q_{new}, which corresponding to the kink effect, is usually unfavorable for the existence of RSAE. We show by both analytic theory and numerical calculation that the artificial suppression of the kink term in the simulation will help to find RSAEs. In the ideal MHD and zero-pressure limit, the main favorable term is the toroidicity term Q_{tor}. Although small, the toroidicity effect Q_{tor} can also excite RSAE under certain parameters. To remove the spurious imaginary frequencies from the ideal MHD modes, we construct a self-adjoint operator for the MHD model equation.

V. ACKNOWLEDGEMENTS

APPENDIX A: THE OPERATOR L

A slight difference between Eqs.(3)-(5) and those in Ref. [12, 14, 16] is that the $L_{m,m\pm1}$ term in this paper is exactly self-adjoint[29] (all eigenvalues ω^2 are real), whereas the $L_{m,m\pm1}$ term in Ref. [12, 14, 16, 23] has broken the self-adjointness of the ideal MHD equation to the order of $O(\epsilon^2)$. The break of the self-adjointness of

the L operator will bring spurious imaginary parts to the eigenvalues. A term $(k_m^2)'$[25, 26] in $L_{m,m}$, coming from the cancelation between the kink term and the field line bending term, is also missed in Ref. [12, 14, 16], which is important for low m modes (see below and Fig.4).

Several test runs for the stable AEs show that the eigenvalues of the self-adjoint equation (3)-(5) are indeed all real numbers, and some small imaginary parts (e.g., 10^{-6}) originated from the discrete errors can be suppressed by using larger N_r. Whereas, the numerical results using the non-self-adjoint equations in Refs. [12, 14, 16, 23] will give artificial non-real eigenvalues. The imaginary parts of those eigenvalues can be large to 10^{-2}, which is consistent with the order of approximation, i.e., $O(\epsilon^2)$. To avoid these non-real solutions, we retain the self-adjointness of Eqs.(3)-(5), though the difference is merely in second order. When the self-adjointness of L is satisfied, we find that a slight difference in the second order term would not affect the results too much. For example, solving the ideal MHD part of Eq.(35) in Ref.[25], which is self-adjoint, will give results similar to those from the AMC code in the zero-β limit. This indicates that the second order approximation is adequate. Fig.4 shows how the inaccurate expressions for L affect the solutions, where a TAE case is solved and the parameters is taken from Ref.[26] (see Appendix C). Panels (a) and (b) give all the solutions using the non-self-adjoint Eq.(82) in Ref.[23] and the self-adjoint MHD part of Eq.(35) in Ref.[25]. We can see that several artificial imaginary frequencies will arise when the self-adjointness is broken. Panels (c) and (d) show the effects of the $(k_m^2)'$ term. When this term is missed, both the mode structure and eigen frequency will be affected. For example, the dominant $m = 1$ mode is shifted outward and concave in panel (c) at range $0 < r < 0.65$ instead of the bulging structure in panel (d) at range $0 < r < 0.57$.

Note also that there exists a sign difference in the definition of $L_{m,m\pm1}$ between Refs.[14] and [16]. This barely affects the solutions, which is mainly because that $L_{m,m+1}$ and $L_{m,m-1}$ are symmetric. However, one should be careful that moving $v_A^2(r)$ out of the ∂_r derivative as in Ref.[16, 21] will break the self-adjointness.

APPENDIX B: DISCRETIZEATION THE SELF-ADJOINT L OPERATOR

The operator $\hat{L}$ in an arbitrary second order ODE $\hat{L}y \equiv a(x)y'' + b(x)y' + c(x)y = \lambda y$, where a, b and c are real functions of x, is not always self-adjoint, i.e., the eigenvalues of the above equation are not always real numbers. However, a self-adjoint Sturm-Liouville operator in the following form always give real eigenvalues

$$\hat{L} = \frac{d}{dx}\Big[f(x)\frac{d}{dx}\Big] + g(x), \qquad (B1)$$

We can discrete this operator properly to an equivalent matrix and to show that the corresponding matrix is self-

TABLE I: Eigenmode frequencies (normalized by $\omega_A = V_A/R_0$) benchmark of AMC with KAEC and NOVA.

		AMC	KAEC	NOVA	-
GAE		1.3842	1.3843	-	-
TAE		0.3107	0.302	0.3127	0.31 (Ref.[26])
TAE	Odd	0.4088	0.4086	0.4050	0.4095 (accu.)
	Even	0.3505	0.3523	0.3550	0.3477 (accu.)

adjoint (Hermitian). Then the linear ODE is transformed to an eigenvalule problem $\boldsymbol{AX} = \lambda\boldsymbol{BX}$ in the matrix form.

For simplicity, the finite difference approach is used to discretize the Sturm-Liouville operator in the form of Eq.(B1), i.e., $L = f_j(y_{j+1} - 2y_j + y_{j-1})/\Delta x^2 + f_j'(y_{j+1} - y_{j-1})/(2\Delta x) + g_j y_j$. The corresponding finite difference matrix is shown to be self-adjoint. Here, the matrix $\boldsymbol{B}$ is unit matrix and can be ignored, whereas $\boldsymbol{A}$ is a real tridiagonal matrix. That is, we need only to show that $\boldsymbol{A}$ is symmetric, i.e, $\boldsymbol{A} = \boldsymbol{A}^T$, or more explicitly, the matrix elements $A_{j,j+1} = A_{j+1,j}$, i.e.,

$$\frac{f_j}{\Delta x^2} + \frac{f_j'}{2\Delta x} = \frac{f_{j+1}}{\Delta x^2} - \frac{f_{j+1}'}{2\Delta x}, \qquad (B2)$$

where the prime is the derivative. Eq.(B2) can be shown to hold to $O(\Delta x^2)$. Therefore, the matrix $\boldsymbol{A}$ is self-adjoint to $O(\Delta x^2)$.

Eq.(6) and the $L_{m,m}$ operator in Eq.(4) are in the Sturm-Liouville form and thus self-adjoint. The self-adjointness of the operator $L_{m,m\pm1}$ in Eq.(5) can be shown in a similar manner.

APPENDIX C: BENCHMARK OF THE AMC CODE

Benchmark of the AMC code is given in this appendix.

Firstly, the global Alfvén eigenmode (GAE) in cylinder geometry is solved by the AMC code and the result is compared to that from the KAEC code[10], with the density profile $\rho = 1.0 - 0.98(r/a)^2$, the safety factor profile $q = 1.001 + 2.0(r/a)^2$, zero-pressure, the toroidal mode number $n = 0$ and the poloidal mode number $m = 2$. The eigenmode frequencies from these two codes agree with each other, i.e., $\omega_{\text{GAE}}^{\text{AMC}} = 1.3842$ and $\omega_{\text{GAE}}^{\text{KAEC}} = 1.3843$[10]. Their mode structures are also similar to each other.

Secondly, the TAE result in Ref.[26] is compared to that from the AMC code. The profiles and parameters are: $q = 1.0 + 1.0(r/a)^2$, $\rho = 1.0$, n=1 and $R_0/a = 4$. The eigenmode frequencies in Ref.[26], and calculated by NOVA, KAEC and AMC are shown in Table I. The radial mode structures [Fig.4(d)] from these codes are also similar. As mentioned, we also find that the $(k_m^2)'$ term we add back in $L_{m,m}$ is important to this low m mode. Otherwise, the frequency and mode structure will not match this well [Fig.4(c)].
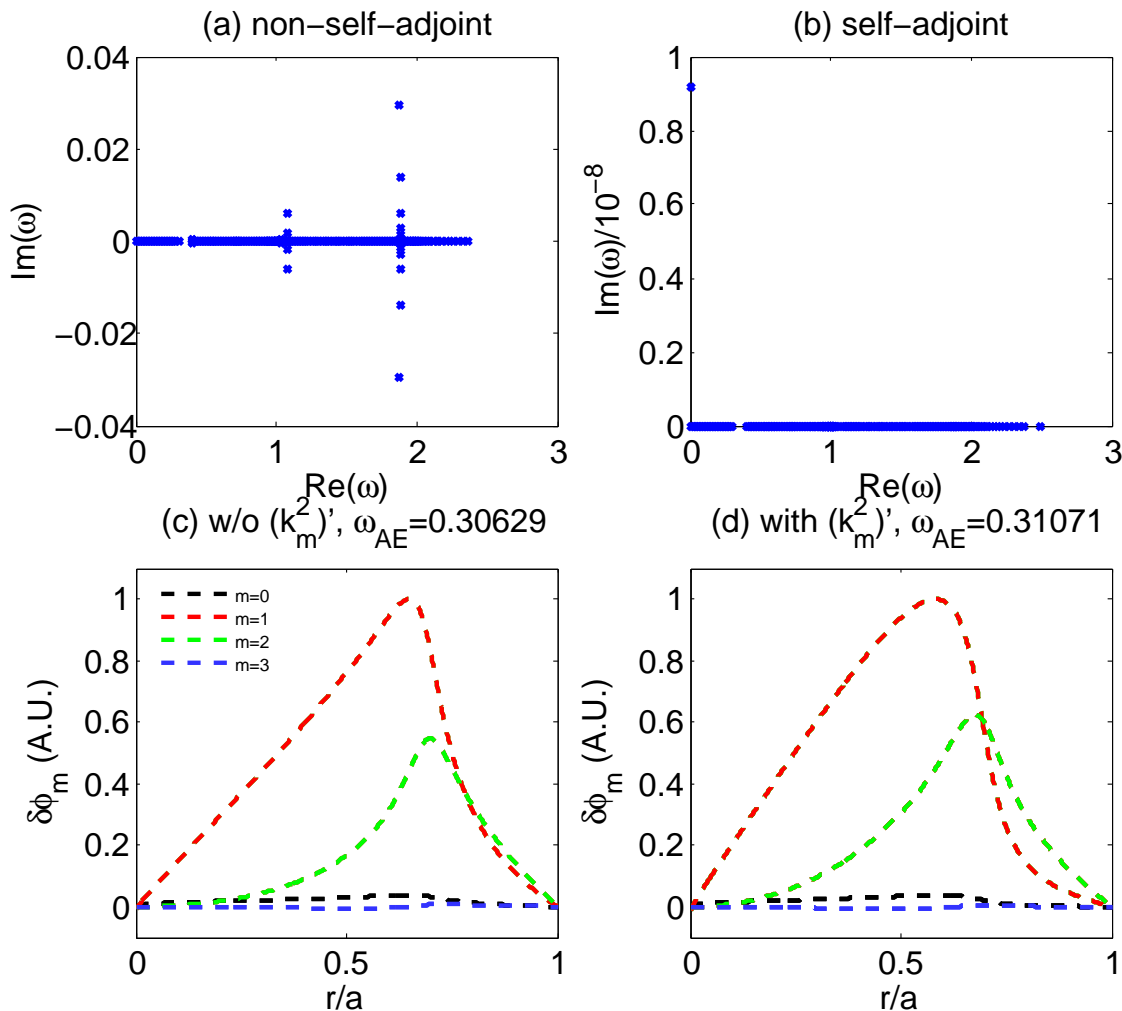
FIG. 4: The effects of the non-self-adjoint L for $n = 1$ TAE mode. Eigen frequencies from (a) the non-self-adjoint Eq.(82) in Ref.[23] and (b) the self-adjoint Eq.(35) in Ref.[25]. Panels (c) and (d) show the radial mode structures and frequency for cases without (Ref.[12, 14, 16]) and with (this paper) $(k_m^2)'$ correction.

We give a further comparison of the odd and even TAEs[28]. The profiles and parameters are: $q = 1.35 + 1.2(r/a)^2$, $\rho = 1/[1 + 2.0(r/a)^2]$, n=1 and $R_0/a = 4$. The odd and even continuum accumulating points (accu.) and eigenmode frequencies calculated by NOVA, KAEC and AMC are also shown in Table I. They are consistent with each other. The continuum spectrum and mode structure calculated by AMC is shown in Fig. 5. From Table I and panel (b) in Fig. 5, we find that the odd eigenmode frequency is slightly below the continuum spectrum and the even eigenmode frequency is slightly

above the continuum spectrum, as expected. The 2D (r, θ) contours in panels (d) and (f) show the ballooning and anti-ballooning structures of even and odd TAEs.

Finally, we have also compared the ideal MHD RSAE results with KAEC in Refs. [10] and [15], and GTC and HMGC in Ref.[20]. Similar mode frequencies and mode structures are obtained, despite some minor differences. In addition, the AMC code has also been successfully applied to the HL-2A experiment for the Alfvén modes[30]. Extending AMC to study the kinetic and collisional effects (e.g., tearing mode) is also under consideration.

[1] S. Sharapov, B. Alper, H. Berk *et al.*, Nucl. Fusion **53**, 104022 (2013).

[2] H. Kimura, Y. Kusama, M. Saigusa, G. J. Kramer, K. Tobita, M. Nemoto, T. Kondoh, T. Nishitani, O. da Costa, T. Ozeki, T. Oikawa, S. Moriyama, A. Morioka, G. Y.

Fu, C. Z. Cheng and V. I. Afanasév, Nucl. Fusion **38**, 1303 (1998).

[3] S. E. Sharapov, D. Testa, B. Alper, D. N. Borba, A. Fasoli, N. C. Hawkes, R. F. Heeter, M. J. Mantsinen and M. von Hellermann, Phys. Lett. A **289**, 127 (2001).
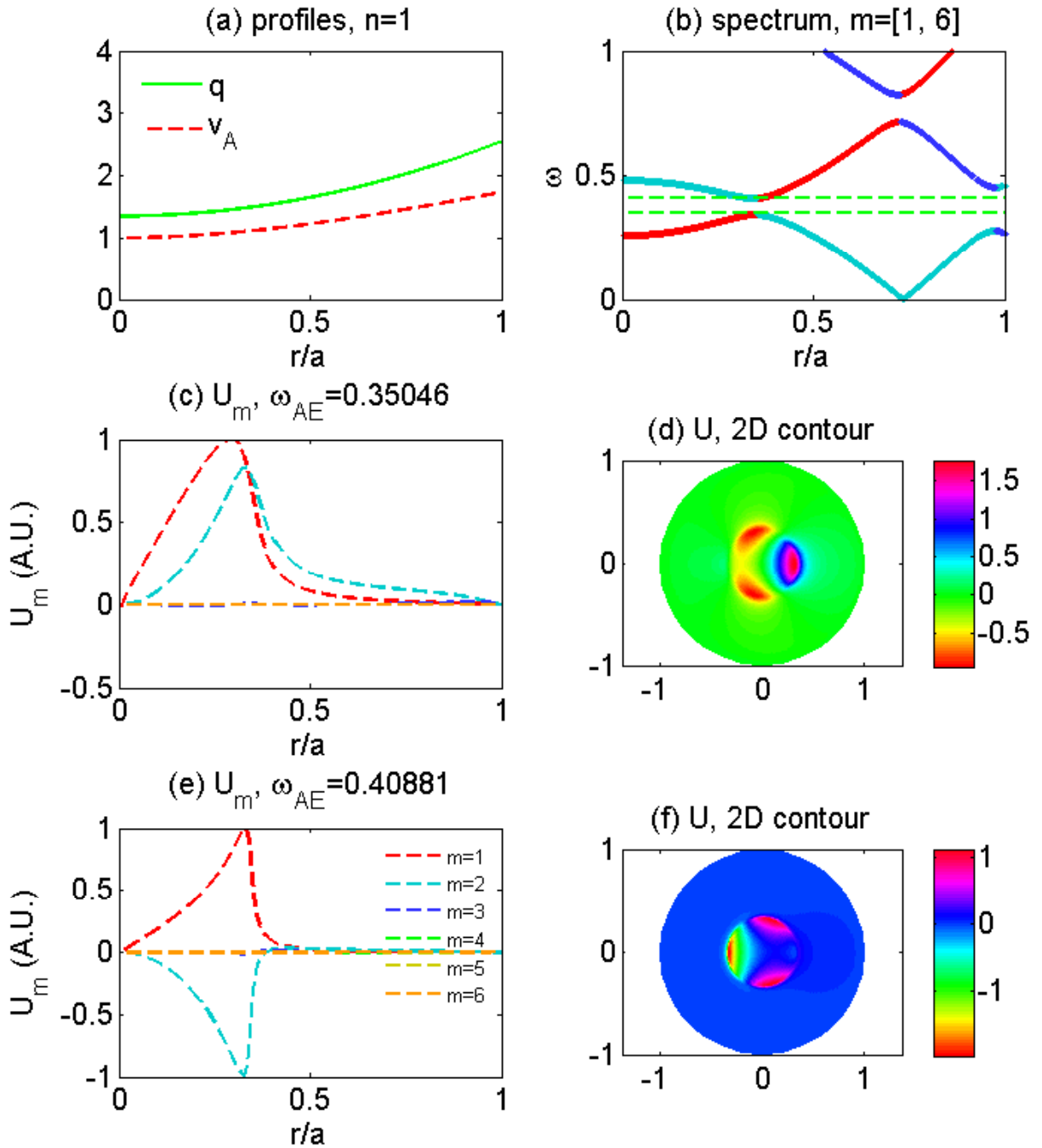
FIG. 5: Odd and even TAEs calculated by AMC are shown under the profiles and parameters $q = 1.35 + 1.2(r/a)^2$, $\rho = 1/[1 + 2.0(r/a)^2]$, n=1 and $R_0/a = 4$.

[4] R. Nazikian, G. J. Kramer, C. Z. Cheng, N. N. Gorelenkov, H. L. Berk, and S. E. Sharapov, Phys. Rev. Lett. **91**, 125003 (2003).

[5] J. A. Snipes, N. Basse, C. Boswell, E. Edlund, A. Fasoli, N. N. Gorelenkov, R. S. Granetz, L. Lin, Y. Lin, R. Parker, M. Porkolab, J. Sears, S. Sharapov, V. Tang and S. Wukitch, Phys. Plasmas **12**, 056102 (2005).

[6] M. A. Van Zeeland, G. J. Kramer, M. E. Austin, R. L. Boivin, W. W. Heidbrink, M. A. Makowski, G. R. McKee, R. Nazikian, W. M. Solomon and G. Wang, Phys.

Rev. Lett. **97**, 135001 (2006).

[7] E. D. Fredrickson, N. A. Crocker, N. N. Gorelenkov, W. W. Heidbrink, S. Kubota, F. M. Levinton, H. Yuh, J. E. Menard and R. E. Bell, Phys. Plasmas **14**, 102510 (2007).

[8] W. Chen, L. M. Yu, Y. Liu, X. T. Ding, H. S. Xie, J. Zhu, L. M. Yu, X. Q. Ji, J. X. Li, Y. G. Li, D. L. Yu, Z. B. Shi, X. M. Song, J. Y. Cao, S. D. Song, Y. B. Dong, W. L. Zhong, M. Jiang, Z. Y. Cui, Y. Huang, Y. Zhou, J. Q. Dong, M. Xu, F. Xia, L. W. Yan, Q. W. Yang, X. R. Duan and HL-2A team, Destabilization of

Reversed Shear Alfvén Eigenmodes Driven by Energetic Ions during NBI in HL-2A plasmas with $q_{\min} \sim 1$, 13th IAEA-TM EP, 17-20 Sep. 2013, Beijing, China, Nuclear Fusion, to appear.

[9] C. Z. Cheng and M. S. Chance, Phys. Fluids **29**, 3695 (1986).

[10] L. M. Yu, G. Y. Fu and Z. M. Sheng, Phys. Plasmas **16**, 072505 (2009).

[11] H. L. Berk, D. N. Borba, B. N. Breizman, S. D. Pinches and S. E. Sharapov, Phys. Rev. Lett., **87**, 185002 (2001).

[12] B. N. Breizman, H. L. Berk, M. S. Pekker, S. D. Pinches and S. E. Sharapov, Phys. Plasmas, **10**, 3649 (2003).

[13] G. J. Kramer, N. N. Gorelenkov, R. Nazikian and C. Z. Cheng, Plasma Phys. Control. Fusion **46**, L23 (2004).

[14] B. N. Breizman, M. S. Pekker and S. E. Sharapov, Phys. Plasmas, **12**, 112506 (2005).

[15] L. M. Yu, X. M. Zhang and Z. M. Sheng, Phys. Plasmas **20**, 082509 (2013).

[16] G. Y. Fu and H. L. Berk, Phys. Plasmas **13**, 052502 (2006).

[17] N. N. Gorelenkov, G. J. Kramer and R. Nazikian, Plasma Phys. Control. Fusion **48**, 1255 (2006).

[18] S. V. Konovalov, A. B. Mikhailovskii, M. S. Shirokov and T. Ozeki, Phys. Plasmas **11**, 2303 (2004).

[19] S. V. Konovalov, A. B. Mikhailovskii, M. S. Shirokov, E. A. Kovalishen and T. Ozeki, Phys. Plasmas **11**, 4531 (2004).

[20] W. Deng, Z. Lin, I. Holod, X. Wang, Y. Xiao and W. Zhang, Phys. Plasmas **17**, 112504 (2010).

[21] W. Deng, Z. Lin and I. Holod, Nucl. Fusion, **52**, 023005 (2012).

[22] F. Zonca, L. Chen and R. A. Santoro, Plasma Phys. Controlled Fusion **38**, 2011 (1996).

[23] G. Vlad, F. Zonca and S. Briguglio, La Rivista del Nuovo Cimento, **22**, 7, pp.1-97 (1999).

[24] Y. Hu, G. Li, N. N. Gorelenkov, H. Cai, W. Yang, D. Zhou and Q. Ren, Phys. Plasmas **21**, 052510 (2014).

[25] H. L. Berk, J. W. van Dam, Z. Guo and D. M. Lindberg, Phys. Fluids B **4**, 1806 (1992).

[26] G. Y. Fu and J. W. van Dam, Phys. Fluids B **1**, 1949 (1989).

[27] H. Wang and Y. Todo, J. Phys. Soc. Jpn. **80**, 094501 (2011).

[28] G. Y. Fu, C. Z. Cheng, R. Budny, Z. Chang, D. S. Darrow, E. Fredrickson, E. Mazzucato, R. Nazikian, K. L. Wong and S. Zweben, Phys. Plasmas **3**, 4036 (1996).

[29] J. P. Freidberg, Rev. Mod. Phys. **54**, 801 (1982).

[30] W. Chen, Z. Qiu, X. T. Ding, H. S. Xie, L. M. Yu, X. Q. Ji, J. X. Li, Y. G. Li, J. Q. Dong, Z. B. Shi, Y. P. Zhang, J. Y. Cao, X. M. Song, S. D. Song, M. Xu, Q. W. Yang, Yi. Liu, L. W. Yan, X. R. Duan and HL-2A team, EPL **107**, 25001 (2014).